ChemComm

COMMUNICATION

View Article Online
View Journal | View Issue

Check for updates

Cite this: *Chem. Commun.*, 2026, **62**, 4050

Received 30th November 2025,
Accepted 26th January 2026

DOI: 10.1039/d5cc06813d

rsc.li/chemcomm

Published on 02 February 2026. Downloaded on 5/22/2026 10:03:05 AM.

Liposome-based delivery of DNA aptamers to inhibit erythromycin methyltransferase-mediated antibiotic resistance

Swagata Patra,* Damini Sahu, Leena L. Badgujar, P. I. Pradeepkumar and Ruchi Anand *

Resistance to macrolides, lincosamides, and the streptogramin B class of antibiotics is caused by the methylation activity of erythromycin methyltransferases. Here, we encapsulated DNA aptamers inhibiting Erm into specifically designed liposomes to enhance stability, uptake, and delivery properties. This delivery system restores erythromycin sensitivity in resistant *Staphylococcus aureus*, offering a promising therapeutic platform against MDR bacteria.

Antibiotic resistance represents a major global health threat, largely driven by the excessive and improper use of antibiotics.[1] One of the most common resistance mechanisms involves structural modifications of antibiotic targets, particularly the bacterial ribosome, the primary site for protein synthesis and a key target for many antibiotics.[2] Methylation and acetylation of ribosomal RNA are the two predominant modification types that hinder drug binding.[3] Several antibiotic classes, including macrolides, lincosamides, and streptogramin B (MLS_B), act by binding to the peptide exit tunnel of the 50S ribosomal subunit, thereby blocking nascent peptide elongation and leading to bacterial cell death.[4] However, methylation of the A2058 residue in 23S rRNA, catalysed by erythromycin resistance methyltransferases (Erms), prevents antibiotic binding and confers resistance.[5] Therefore, inhibiting Erm-mediated methylation presents a promising strategy to combat bacterial resistance and restore the efficacy of key antibiotics.

Several strategies have been explored to inhibit Erm,[6] primarily through high-throughput virtual and experimental screening of small molecules targeting the conserved SAM-binding site of Erms.[7] Peptide inhibitors identified *via* phage display have also shown potential.[8] However, SAM-site inhibitors often risk off-target effects due to structural similarity among methyltransferases, and RNA-site binders lack specificity. To counter problems of limited specificity, SELEX-based aptamers serve as an alternative to traditional drug design methods. For instance, several aptamers have been developed that effectively recognize mammalian cancer cells, such as colorectal and leukemia cell types.[9,10] Moreover, aptamers offer key advantages over antibodies, including low immunogenicity, ease of synthesis, batch consistency, reversible folding, and tunable pharmacological properties.[11] They can also function effectively under extreme physiological conditions. The intracellular delivery of this aptamer in a pathogenic bacterial strain has always been a challenging task. Since nucleic acids are very charged molecules, they often face severe delivery problems in live cells. Methods such as lipofectin and electroporation have been tried in the past, but they result in either low delivery percentage or in damaging the cell structure during entry, and are generally not practical approaches in a clinical setting. Therefore, more feasible and biocompatible delivery systems are currently being used. The advent of nucleic acid vaccine technologies has advanced the field, and an efficient delivery methodology in mammalian cells has seen a surge of development. For instance, for efficient and safe transport of DNA and RNA molecules, delivery systems including viral vectors, lipid-based carriers, polymeric nanoparticles, liposomes, lipid nanoparticles (LNPs), peptide-based systems, and inorganic nanoparticles such as gold or silica-based carriers have been developed.[12,13] However, only a few of these studies are targeted towards efficient delivery in the bacterial system.[14,15] Therefore, in this report, we used a recently discovered DNA aptamer highly specific for Erm42[16] (Fig. S1a), an Erm found in pathogen *Mannheimia haemolytica* and *Pasteurella multicoda*, and show that liposomes are an ideal delivery vehicle. This was chosen as the preferred platform, owing to its established clinical viability, ability to effectively encapsulate nucleic acids, protect them from enzymatic degradation, and facilitate efficient cellular uptake. Here, we show that this delivery system efficiently reverses Erm-mediated resistance in MDR *S. aureus*.

Liposomes were prepared using a lipid mixture of (2,3-dioleoyloxy-propyl)-trimethylammonium-chloride (DOTAP),

Department of Chemistry, Indian Institute of Technology Bombay, Mumbai, India. E-mail: swagata1012@gmail.com, ruchi@chem.iitb.ac.in

This journal is © The Royal Society of Chemistry 2026

Published on 02 February 2026. Downloaded on 5/22/2026 10:03:05 AM.

1,2-dioleoyl-*sn-glycero*-3-phosphoethanolamine (DOPE), 1,2-distearoyl-*sn-glycero*-3-phosphoethanolamine-*N*(methoxy(polyethyleneglycol)-2000) (DSPE–PEG) (Fig. S1b) using the conventional thin-film hydration method (Fig. S2).[14] Here, DOTAP imparts a positive charge to facilitate electrostatic interaction with negatively charged DNA aptamers, while DOPE enhances membrane fusion and cellular uptake, and DSPE–PEG improves liposome stability, biocompatibility, and circulation time under physiological conditions.[15] The liposome formulations were characterized using dynamic light scattering (DLS) to assess particle size and dispersity, UV-vis spectroscopy to confirm DNA incorporation (Fig. 1). Different liposomal formulations were prepared using varying lipid concentrations. LP1 and LP5 correspond to 1 mM and 5 mM total lipids, respectively. The aptamer-loaded formulations—LP1/N1, LP1/N2, LP5/N1, and LP5/N2 represent liposomes containing 1 μM and 2 μM aptamer at the corresponding lipid concentrations (Fig. 1A). LP5 exhibited a hydrodynamic diameter of 170 ± 20 nm, a PDI of 0.21 ± 0.03, and a zeta potential of +17 ± 3 mV (Table S1). The incorporation of DNA aptamers (LP5/N2) did not alter the vesicle size (Fig. 1B). However, increasing the aptamer concentration progressively reduced the surface charge, likely due to electrostatic interactions between the negatively charged aptamer and the cationic liposome surface. All formulations maintained polydispersity index (PDI) values below 0.23, confirming the formation of small, monodispersed vesicles. The influence of the aptamer concentration (1 μM and 2 μM) on encapsulation efficiency (%EE) was also evaluated (Table S1), and it showed above 50%. To confirm cellular uptake or membrane association without altering their physicochemical properties, liposomes were labelled with a rhodamine derivative (Rh-DHPE). This enables fluorescence-based visualization and tracking (Fig. S3). The resulting Rh-LP formulations exhibited hydrodynamic diameters of 161–165 nm, PDI values of 0.20–0.23, and zeta potentials of +15 to +17 mV, closely matching those of their corresponding unloaded LP5 formulation, confirming that fluorescent labeling did not impact liposome characteristics.

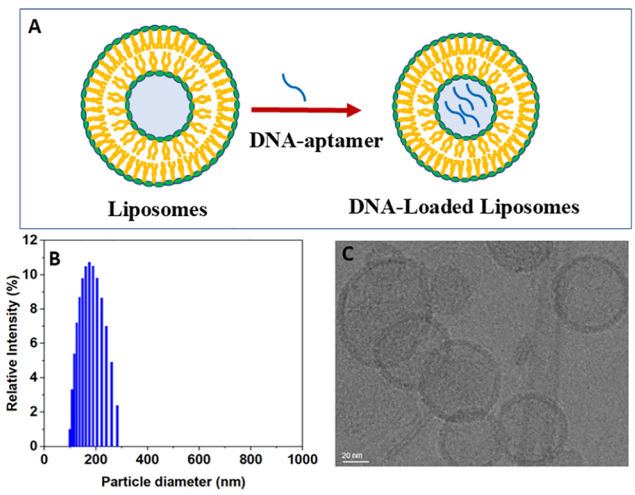

Fig. 1 (A) Schematic representation of DNA aptamer loaded liposomes prepared using DOTAP, DOPE, and DSPE–PEG at 1 mM (LP1) and 5 mM (LP5) total lipid concentration, with aptamer concentrations of 1 μM (N1) and 2 μM (N2). (B) Particle size distribution of LP5/N2, (C) Cryo-TEM micrograph of DNA-loaded liposomes (LP5/N2).

The morphology of the liposomes was examined using cryo-TEM (Fig. 1C). The cryo-TEM image of DNA-loaded liposomes (LP5/N2) revealed the formation of well-defined spherical vesicles with diameters in the range of 45–60 nm (Fig. 1C).

It is important to note that the mean hydrodynamic diameter obtained from DLS measurements is larger than the size observed in cryo-TEM images. This discrepancy arises because DLS measures the hydrodynamic diameter of liposomes in their hydrated state, accounting for the solvation shell and Brownian motion in the aqueous medium, whereas cryo-TEM provides the physical diameter of particles under vacuum conditions.[17]

The interaction between cationic liposomes and Gram-positive bacteria was further analysed by flow cytometry following exposure to rhodamine-labeled liposomes. After incubation, samples were washed with 0.1% (v/v) detergent to remove liposomes adsorbed.[18] Fusion efficiency was determined by quantifying the percentage of fluorescently stained cells. To assess lipid dose dependence, bacterial cells were treated with increasing concentrations of DOTAP/DOPE/DSPE–PEG liposomes while maintaining a constant rhodamine level (Fig. S3). At 1 mM lipid concentration, only 28% of resistant *S. aureus* cells were stained, whereas at 5 mM, fusion efficiency dramatically increased to 99%. These results demonstrate that lipid concentration strongly influences the membrane fusion of DOTAP/DOPE/DSPE–PEG liposomes with bacteria. Confocal laser scanning microscopy (CLSM) confirmed the presence of fluorescent lipids within the bacterial cytosol (Fig. S4), validating the successful fusion and internalization of the cationic liposomes.

The intracellular delivery of the aptamer into resistant *S. aureus* was evaluated using flow cytometry (Fig. 2A–D). Different lipid and aptamer concentrations were tested by incubating bacteria with liposomal formulations, 1 mM liposomes containing 1 μM and 2 μM aptamer (LP1/N1 and LP1/N2, respectively) and 5 mM liposomes containing 1 μM and 2 μM aptamer (LP5/N1 and LP5/N2, respectively). Since free DNA aptamers are unable to penetrate the bacterial envelope due to their large molecular size and negative charge, negligible fluorescence was observed when the free aptamer was incubated with bacteria. In contrast, aptamer-loaded liposomes demonstrated a significantly higher percentage of fluorescently stained cells, confirming successful internalization. Increasing lipid concentrations (from LP1/N1 to LP5/N1) led to higher intracellular fluorescently stained cells (10% to 84%), indicating improved membrane fusion and enhanced uptake (Fig. 2E). Similarly, higher aptamer concentrations in the formulation (from LP5/N1 to LP5/N2) resulted in increased delivery efficiency from 84% to 97%. CLSM further confirmed the cytosolic delivery of DNA aptamers. After treatment with DNA-loaded liposomes, bacterial cells were counterstained with DAPI, revealing colocalization of DAPI and FAM-labeled aptamer

Published on 02 February 2026. Downloaded on 5/22/2026 10:03:05 AM.

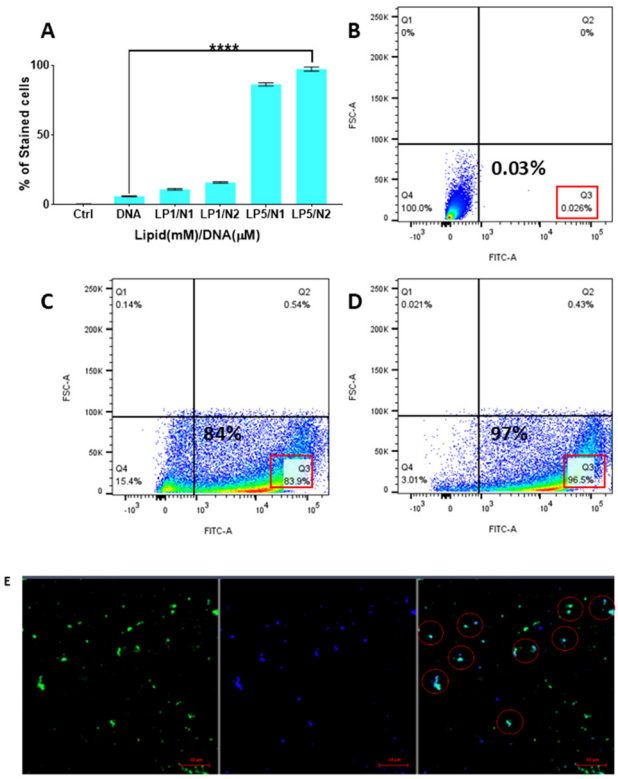

Fig. 2 Cellular internalization of DNA-loaded liposome in resistant *S. aureus*. (A) Quantitative analysis of FAM-labeled DNA aptamer uptake by flow cytometry showing a dose-dependent increase in the percentage of stained cells with increasing lipid and DNA concentrations (LP1/N1 = 1 mM lipid + 1 μM DNA; LP1/N2 = 1 mM lipid + 2 μM DNA; LP5/N1 = 5 mM lipid + 1 μM DNA; LP5/N2 = 5 mM lipid + 2 μM DNA) after 2 h incubation. A Dunnett's multiple comparison test (ANOVA one-way) was used to establish statistical significance. Sign [$p \leq 0.0001$(****), $p \leq 0.001$(***), $p \leq 0.01$(**), $p \leq 0.1$(*)] indicates a significant difference, and ns means not a significant difference. (B) Flow cytometry of untreated control cells showing negligible fluorescence (0.03%), (C) cells treated with 5 mM lipid and 1 μM FAM-DNA liposomes (LP5/N1) show strong fluorescence, indicating 84% internalization, (D) cells treated with 5 mM lipid and 2 μM FAM-DNA liposomes (LP5/N2) show strong fluorescence, indicating 97% internalization. (E) Confocal microscopy images confirming intracellular localization of FAM-labeled DNA (green) within DAPI-stained bacterial cells (blue); merged image highlights co-localization (red circles).

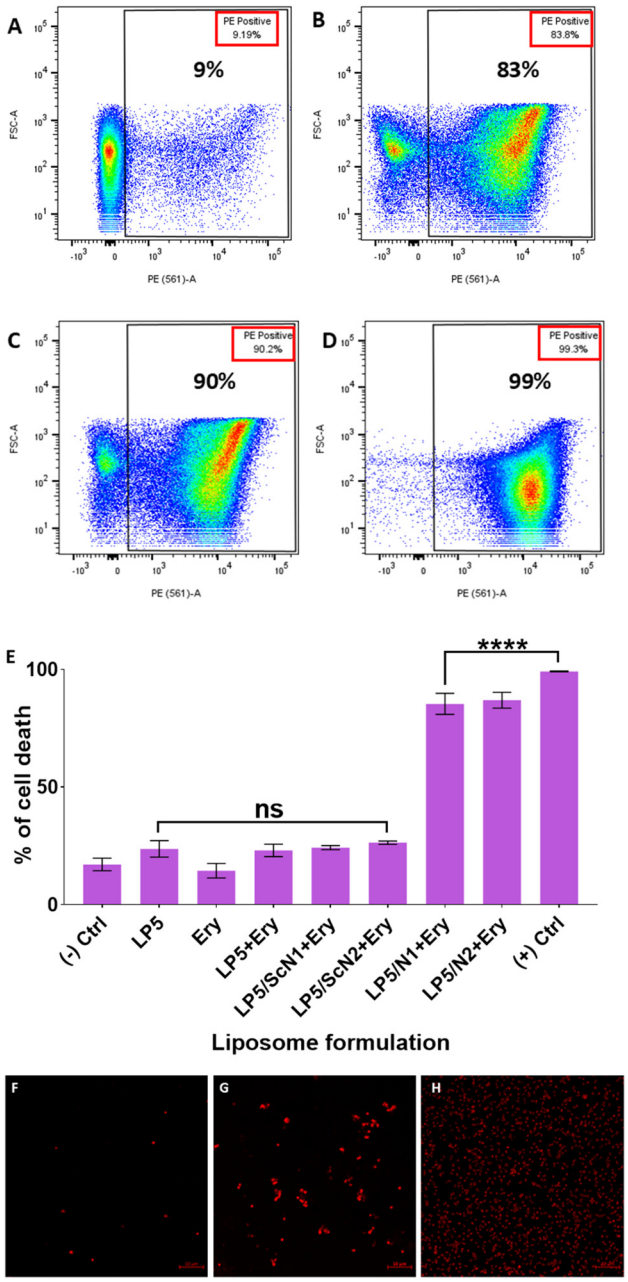

Fig. 3 Evaluation of bactericidal activity of aptamer-loaded liposomes against resistant *S. aureus*. (A)–(D) Representative flow cytometry plots showing the percentage of dead cells for (A) Ery, (B) LP5/N1 + Ery, (C) LP5/N2 + Ery, and (D) positive control, heat-inactivated dead cells respectively. (E) Quantitative analysis of cell death by flow cytometry after treatment with various formulations. LP5, Ery alone, and (LP5/ScN1 or LP5/ScN2 + Ery) showed minimal killing, while aptamer-loaded liposomes (LP5/N1 + Ery and LP5/N2 + Ery) exhibited significantly enhanced bacterial cell death. A Dunnett's multiple comparison test (ANOVA one-way) was used to establish statistical significance. Sign [$p \leq 0.0001$(****), $p \leq 0.001$(***), $p \leq 0.01$(**), $p \leq 0.1$(*)] indicates a significant difference, and ns means not a significant difference. (F)–(H) Confocal microscopy images of dead cells for (F) Ery, (G) LP5/N2 + Ery, and (H) positive control, respectively.

signals (Fig. 2F–H). This overlap confirmed that liposomes effectively fused with the bacterial membrane and released the aptamer into the cells, where it can interact with the intracellular target, Erm. Wild-type *S. aureus* was also used as a control (Fig. S5), confirming efficient bacterial uptake by the liposomal system.

To evaluate the cytotoxic effects of liposomal formulations and the cell viability of aptamer-loaded liposomes, propidium iodide (PI) staining flow cytometry and confocal microscopy was used (Fig. 3 and Table S2). The 5 mM liposomal formulations showed only a slight increase in cytotoxicity, and treatment with erythromycin (Ery) with liposome formulations did not produce appreciable cell death (Fig. 3 and Fig. S6). In resistant *S. aureus*, Ery alone did not induce cell death; however, in the presence of the aptamer, cell killing increased to 84% with LP5/N1, and with LP5/N2, cell death reached 90%. Confocal microscopy imaging confirmed these findings by showing a strong increase in PI-positive (dead) bacterial cells

 This journal is © The Royal Society of Chemistry 2026

Published on 02 February 2026. Downloaded on 5/22/2026 10:03:05 AM.

when treated with aptamer-loaded liposomes (Fig. 3). While erythromycin alone showed minimal cell death, the LP5/N2 formulations produced intense red fluorescence, indicating significantly higher bacterial killing due to aptamer-mediated action (Fig. 3). Increasing DNA aptamer loading in LP5 formulations (0.5 μM to 2 μM) led to a clear dose-dependent enhancement of erythromycin-mediated bacterial killing, with maximal cell death observed at the highest aptamer concentration, supporting an aptamer-driven mechanism (Fig. S7 and Table S2). Further, to check the authenticity of specificity of the Erm aptamer a scrambled DNA aptamer control was also included. Flow cytometry analysis demonstrated that treatment with scrambled DNA–loaded liposomes (LP5/ScN1 or LP5/ScN2), in combination with Ery, did not result in significant bacterial cell death (Fig. 3 and Fig. S8). These results indicate that the aptamer binds to and inhibits the Erm methyltransferase responsible for methylation mediate erythromycin resistance. By blocking Erm-mediated methylation of rRNA, the aptamer prevents modification of the antibiotic binding site, allowing erythromycin to effectively bind the ribosome again and restore its antibacterial activity against resistant *S. aureus*.

In conclusion, this study demonstrated an aptamer-based strategy to overcome erythromycin resistance in MDR *S. aureus* by specifically targeting the Erm enzyme using a liposome-based delivery system. To enhance intracellular delivery, a DOTAP/DOPE/DSPE–PEG liposome formation was optimized, which effectively protected the aptamer from enzymatic degradation and enhanced cellular uptake. Importantly, incorporation of DOPE reduced cationic toxicity while maintaining delivery efficiency. Flow cytometry and CLSM demonstrated efficient membrane fusion and cytoplasmic release of aptamers in resistant *S. aureus*. The combination with aptamer-loaded liposomes restored antibiotic efficacy, resulting in up to 90% cell death. These findings confirm that aptamers developed for specific resistance-expressing proteins can serve as a viable route to reverse resistance. Here, pre-existing antibiotics in combination with an engineered aptamer can be used to combat drug resistance. This liposome-based aptamer delivery approach offers a clinically viable and versatile platform to combat antibiotic resistance and opens avenues to be adapted to target other resistance mechanisms or bacterial pathogens.

Conflicts of interest

There are no conflicts to declare.

Data availability

The data supporting this article have been included as part of the supplementary information (SI). Supplementary information is available. See DOI: https://doi.org/10.1039/d5cc06813d.

Acknowledgements

This work was financially supported by the Scheme for Transformational and Advanced Research in Sciences (STARS), Ministry of Education, Government of India (grant no. MoE STARS/STARS1/523). The authors would like to thank the ANRF and the IoE-supported national cryo-EM facility at IIT Bombay, flow cytometery, and the confocal Microscopy central facility at IIT Bombay. R. A. acknowledges DBT/Wellcome Trust India Alliance (IA/S/19/1/504293). S. P. acknowledges IIT Bombay for the Institute Postdoctoral Fellowship, D. S. thanks Prime Minister's Research Fellowship (PMRF) for the PhD fellowships, L. L. B. thanks DST-INSPIRE. We thank Ms Shivalika Sharma and Mr Pratik Shetye for their assistance with DLS measurements and flow cytometry experiments.

References

1 A. Abbas, A. Barkhouse, D. Hackenberger and G. D. Wright, *Cell Host Microbe*, 2024, **32**(6), 837–851.
2 A. J. Schaenzer and G. D. Wright, *Trends Mol. Med.*, 2020, **26**, 768–782.
3 L. Jeremia, B. E. Deprez, D. Dey, G. L. Conn and W. M. Wuest, *RSC Med. Chem.*, 2023, **14**, 624–643.
4 T. Tenson, M. Lovmar and M. Ehrenberg, *J. Mol. Biol.*, 2003, **330**, 1005–1014.
5 M. S. Svetlov, E. A. Syroegin, E. V. Aleksandrova, G. C. Atkinson, S. T. Gregory, A. S. Mankin and Y. S. Polikanov, *Nat. Chem. Biol.*, 2021, **17**, 412–420.
6 I. P. Foik, I. Tuszynska, M. Feder, E. Purta, F. Stefaniak and J. M. Bujnicki, *Eur. J. Med. Chem.*, 2018, **146**, 60–67.
7 S. Hanessian and P. W. M. Sgarbi, *Bioorg. Med. Chem. Lett.*, 2000, **10**(5), 433–437.
8 R. B. Giannattasio and B. Weisblum, *Antimicrob. Agents Chemother.*, 2000, **44**(7), 1961–1963.
9 Y. Kwon, M. Lee, N. K. Kaushik, H. Y. Yoo, C. Park, M.-H. Lee and T. Lee, *Chem. Eng. J.*, 2025, **506**, 159935.
10 K. G. Earnest, E. M. McConnell, E. M. Hassan, M. Wunderlich, B. Hosseinpour, B. S. Bono, M. J. Chee, J. C. Mulloy, W. G. Willmore, M. C. DeRosa and E. J. Merino, *Sci. Rep.*, 2021, **11**, 19174.
11 S. Ni, Z. Zhuo, Y. Pan, Y. Yu, F. Li, J. Liu, L. Wang, X. Wu, D. Li, Y. Wan, L. Zhang, Z. Yang, B.-T. Zhang, A. Lu and G. Zhang, *ACS Appl. Mater. Interfaces*, 2021, **13**, 9500–9519.
12 M. J. Beha, J. S. Ryu, Y. S. Kim and H. J. Chung, *Mater. Sci. Eng., C*, 2021, **126**, 112167.
13 X. Peng, J. Chen, Y. Gan, L. Yang, Y. Luo, C. Bu, Y. Huang, X. Chen, J. Tan, Y. Y. Yang and P. Yuan, *Sci. Adv.*, 2024, **10**(14), 9754.
14 S. Pereira, R. S. Santos, L. Moreira, N. Guimarães, M. Gomes, H. Zhang, K. Remaut, K. Braeckmans, S. De Smedt and N. F. Azevedo, *Pharmaceutics*, 2021, **13**, 989.
15 L. Moreira, N. M. Guimarães, S. Pereira, R. S. Santos, J. A. Loureiro, M. C. Pereira and N. F. Azevedo, *ACS Infect. Dis.*, 2022, **8**, 1218–1230.
16 L. Badgujar, D. Sahu, R. Anand and P. I. Pradeepkuma, *ACS Infect. Dis.*, 2026, **12**, 212–223.
17 B. Kim, H. W. Seo, K. Lee, D. Yong, Y. K. Park, Y. Lee, S. Lee, D.-W. Kim, D. Kim and C.-M. Ryu, *Adv. Healthcare Mater.*, 2025, **14**, e2403281.
18 K. Buyens, S. C. De Smedt, K. Braeckmans, J. Demeester, L. Peeters, L. A. van Grunsven, X. de Mollerat du Jeu, R. Sawant, V. Torchilin, K. Farkasova, M. Ogris and N. N. Sanders, *J. Controlled Release*, 2012, **158**, 362–370.